Acta Oceanol. Sin., 2019, Vol. 38, No. 4, P. 29–38
https://doi.org/10.1007/s13131-018-1222-4
http://www.hyxb.org.cn
E-mail: hyxbe@263.net

Seasonal characteristics and formation mechanism of the thermohaline structure of mesoscale eddy in the South China Sea

Yongcan Zu[1, 2], Shuangwen Sun[2, 3*], Wei Zhao[1], Peiliang Li[4], Baochao Liu[2], Yue Fang[2, 3], Azizan Abu Samah[5]

[1] College of Oceanic and Atmospheric Sciences, Ocean University of China, Qingdao 266100, China

[2] Center for Ocean and Climate Research, First Institute of Oceanography, Ministry of Natural Resources, Qingdao 266061, China

[3] Laboratory for Regional Oceanography and Numerical Modeling, Pilot National Laboratory for Marine Science and Technology (Qingdao), Qingdao 266237, China

[4] Ocean College, Zhejiang University, Zhoushan 316021, China

[5] Institute of Ocean and Earth Sciences, University of Malaya, Kuala Lumpur 50603, Malaysia

Received 8 March 2018; accepted 10 May 2018

Abstract

The seasonal characteristics and formation mechanism of the thermohaline structure of mesoscale eddy in the South China Sea are investigated using the latest eddy dataset and ARMOR3D data. Eddy-centric composites reveal that the horizontal distribution of temperature anomaly associated with eddy in winter is more of a dipole pattern in upper 50 m and tends to be centrosymmetric below 50 m, while in summer the distribution pattern is centrosymmetric in the entire water column. The horizontal distribution of eddy-induced salinity anomaly exhibits similar seasonal characteristics, except that the asymmetry of the salinity anomaly is weaker. The vertical distribution of temperature anomaly associated with eddy shows a monolayer structure, while the salinity anomaly demonstrates a triple-layer structure. Further analysis indicates that the vertical distribution of the anomalies is related to the vertical structure of background temperature and salinity fields, and the asymmetry of the anomalies in upper 50 m is mainly caused by the horizontal advection of background temperature and salinity.

Key words: mesoscale eddy, thermohaline structure, seasonal characteristics, South China Sea

Citation: Zu Yongcan, Sun Shuangwen, Zhao Wei, Li Peiliang, Liu Baochao, Fang Yue, Samah Azizan Abu. 2019. Seasonal characteristics and formation mechanism of the thermohaline structure of mesoscale eddy in the South China Sea. Acta Oceanologica Sinica, 38(4): 29–38, doi: 10.1007/s13131-018-1222-4

1 Introduction

Eddy is a widespread mesoscale phenomenon in oceans with horizontal scale of tens to hundreds of kilometers and duration ranging from days to months (Chelton et al., 2007, 2011; Faghmous et al., 2015). Since most eddies rotate faster than their propagation speed (Chelton et al., 2011), they can capture a large volume of water during their migration and constantly keep the water moving, and thus play an important role in mass and energy transport (Zhang et al., 2014; Dong et al., 2014). In addition, eddy also has significant impacts on local horizontal and vertical distribution of marine substances through its primary physical processes such as stirring and pumping (Gaube et al., 2014). Eddy pumping can induce strong vertical exchange of many oceanic tracers (e.g., temperature, salinity, nutrients), causing rapid change in vertical distribution (Klein and Lapeyre, 2009), which may vary from region to region. For example, the salinity anomaly caused by eddy pumping shows a positive-negative double-layer vertical structure in the Southern Ocean (Frenger et al., 2015), but a monolayer vertical structure in the North Atlantic subtropical gyre (Amores et al., 2017a). The effects of eddy stirring and pumping have important implications on the air-sea interaction over eddy (Small et al., 2008) and marine organism inside eddy (Falkowski et al., 1991).

The South China Sea (SCS), the largest semi-enclosed marginal sea in the northwestern Pacific Ocean, is dominated by monsoon, and its circulation and temperature and salinity (TS) distribution have distinct seasonal characteristics (Wyrtki, 1961; Fang et al., 1996; Fang et al., 2012). The unique geographical feature and seasonal variation of environment dynamics make the eddies in the SCS quite different from those in open oceans (Wang et al., 2008; Zu et al., 2013; Chen et al., 2015), in particular the structure of eddy-induced TS anomaly. As illustrated by Sun et al. (2016), the horizontal distribution of eddy-induced sea surface temperature (SST) anomaly in the SCS presents a dipole pattern in winter and a monopole pattern in summer, and the accompanying local wind anomaly show similar seasonal pattern because of ocean-atmosphere coupling. However, their study focuses only on eddy-induced temperature anomaly at sea surface,

Foundation item: The National Key R&D Program of China under contract No. 2017YFC1405100; the National Natural Science Foundation of China under contract Nos 41576028, 41306032 and 41876030; the NSFC-Shandong Joint Fund for Marine Science Research Centers under contract No. U1606405; the research fund from FIO-UM Joint Center of Marine Science and Technology.
*Corresponding author, E-mail: ssun@fio.org.cn

the anomalies below the surface and their seasonality are not clear yet. Other previous studies tried to reveal the three-dimensional structure of the eddy in the SCS, but all of them are mainly of case analysis (Huang et al., 2010; Nan et al., 2011; Hu et al., 2011; Hu et al., 2014; Wang et al., 2015; Shu et al., 2016; Zhang et al., 2016). Therefore, uncertainties still exist in our knowledge on general thermohaline structure of the eddies in the SCS.

In this paper, we investigate the seasonal characteristics of thermohaline structure associated with eddy in the SCS and explore its mechanism on basis of reconstructed observations. Section 2 introduces the datasets and methods to be used in this study. Section 3 illustrates the seasonal characteristics of TS anomaly associated with eddies through composite maps. In Section 4, mechanism of the formation of thermohaline structure will be proposed. A summary is presented in Section 5.

2 Data and methods

2.1 *Data*

The eddy dataset used in this study is from Mesoscale Eddy Trajectory Atlas Product, which is distributed by Archiving, Validation, and Interpretation of Satellite Oceanographic (AVISO). The dataset is upgraded with better eddy tracking algorithm from the fourth version of the eddy database provided by Chelton et al. (2011). In addition to the tracks of eddies detected and monitored on basis of daily gridded sea level anomaly (SLA) fields, information such as eddy centers, radii, amplitudes, rotational velocities, and polarities are also included in the dataset. The definitions of eddy radius and amplitude can be found in Chelton et al. (2011). To avoid noise signal, eddies, whose lifetime is shorter than 28 d or amplitude is smaller than 1 cm, are excluded in our analysis.

The TS and geostrophic currents used for analysis are from the latest (Version 4) Global ARMOR3D L4 Reprocessed dataset (ARMOR3D) offered by Copernicus Marine Environment Monitoring Service (CMEMS). The dataset synthesizes historical satellite measurements (SLA, geostrophic surface currents, SST) and *in-situ* observations, its weekly three-dimensional TS fields have a horizontal resolution of 0.25°×0.25° and vertical resolution ranging from 10 to 100 m (totally 19 levels in vertical in upper 1 000 m) (Guinehut et al., 2004, 2012). Compare to the old version, the new one has higher spatial resolution and accuracy. The 3-D geostrophic currents and geopotential heights are computed from the ARMOR3D T/S fields and surface geostrophic currents through thermal wind equation referenced at sea surface (Mulet et al., 2012). The gridded ARMOR3D data can well distinguish mesoscale eddy signal in space and have been used for eddy compositing in previous studies (e.g., Mason et al., 2017).

2.2 *Methods*

All the eddies in 1993 to 2016 in the area (10°–24°N, 110°–120°E) deeper than 1 000 m are included in analysis. There are 3 859 anticyclonic eddies (AEs) and 3 978 cyclonic eddies (CEs) in total, and their locations are shown in Fig. 1. High eddy activities are found along the northwestern continental shelf and in the deep region west to the Luzon Island, consistent with the results of previous studies (Chen et al., 2011; Sun et al., 2016). In order to investigate the seasonal differences in thermohaline structure of eddies, eddies in DJF (December, January and February) and JJA (June, July and August) are selected for composite analysis of winter and summer, respectively. Totally, there are 962 AEs and 925 CEs in winter, 1 012 AEs and 1 028 CEs in summer, with average amplitude of ~8 cm and radius of ~100 km (Table 1).

We first calculate TS anomalies by subtracting seasonal variation from the original TS data. Then a 3-week low-pass filter is applied to the time series of TS anomalies at each grid point to remove weather-related high-frequency variations. However, the obtained TS anomaly fields consist of not only mesoscale anomalies associated with eddies that we are interested, but also large-scale variability related to ocean circulation. Therefore, a 2°×2° spatial high-pass filter is further applied to the obtained TS anomaly fields. The above data filtering process can well extract eddy signals from the original TS data (Sun et al., 2016). Same filtering strategy is used to derive the anomalous currents associated with eddies from geostrophic current data of the ARMOR3D. Following the composite method by Amores et al. (2017b), 2°×2° fields are extracted from the obtained TS and current anomalies at the center of each eddy, then eddy composite maps can be obtained separately by averaging the extracted fields by seasons (winter or summer) and eddy types (AEs or CEs).

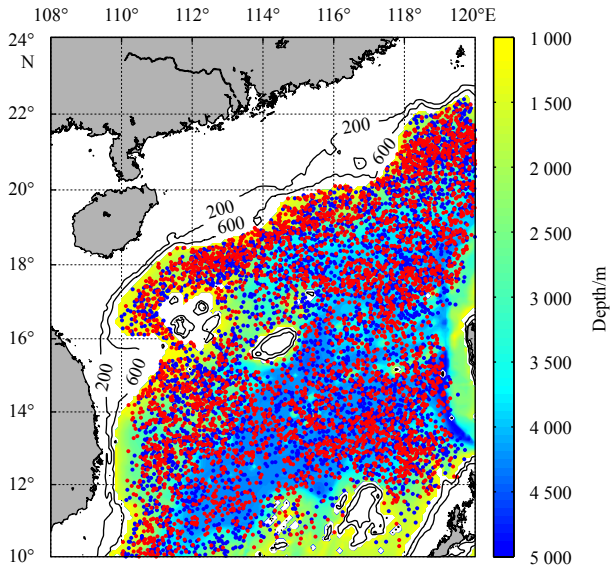

Fig. 1. Locations of all the eddies in 1993 to 2016 in the region with water depth greater than 1 000 m. Red and blue dots denote AEs (3 859) and CEs (3 978), respectively. Black lines are isobaths of 200 m and 600 m.

Table 1. The number, average amplitude and average radius of eddies in winter and summer

	Number		Amplitude/cm		Radius/km	
	CE	AE	CE	AE	CE	AE
Winter (DJF)	925	962	7.6	8.4	98	99
Summer (JJA)	1 028	1 012	6.8	9.2	94	111

3 Seasonal characteristics of thermohaline structure

3.1 *Temperature structure*

Composite maps of eddy-induced temperature anomalies are shown in Figs 2 and 3. One can see that, the maximal values of the anomalies in summer are located close to the center of eddy, and distribution patterns of the anomalies are largely centrosymmetric. In winter, however, the symmetry of the temperature anomalies is retained only in the layers at 100 m or deeper. For the layers shallower than 100 m (i.e., 0 m, 20 m, 50 m), the location of maximum anomaly in each layer deviates further and further away from eddy center as water depth decreases. This feature is particularly obvious for AEs (Figs 2a–c). At sea surface, warm an-

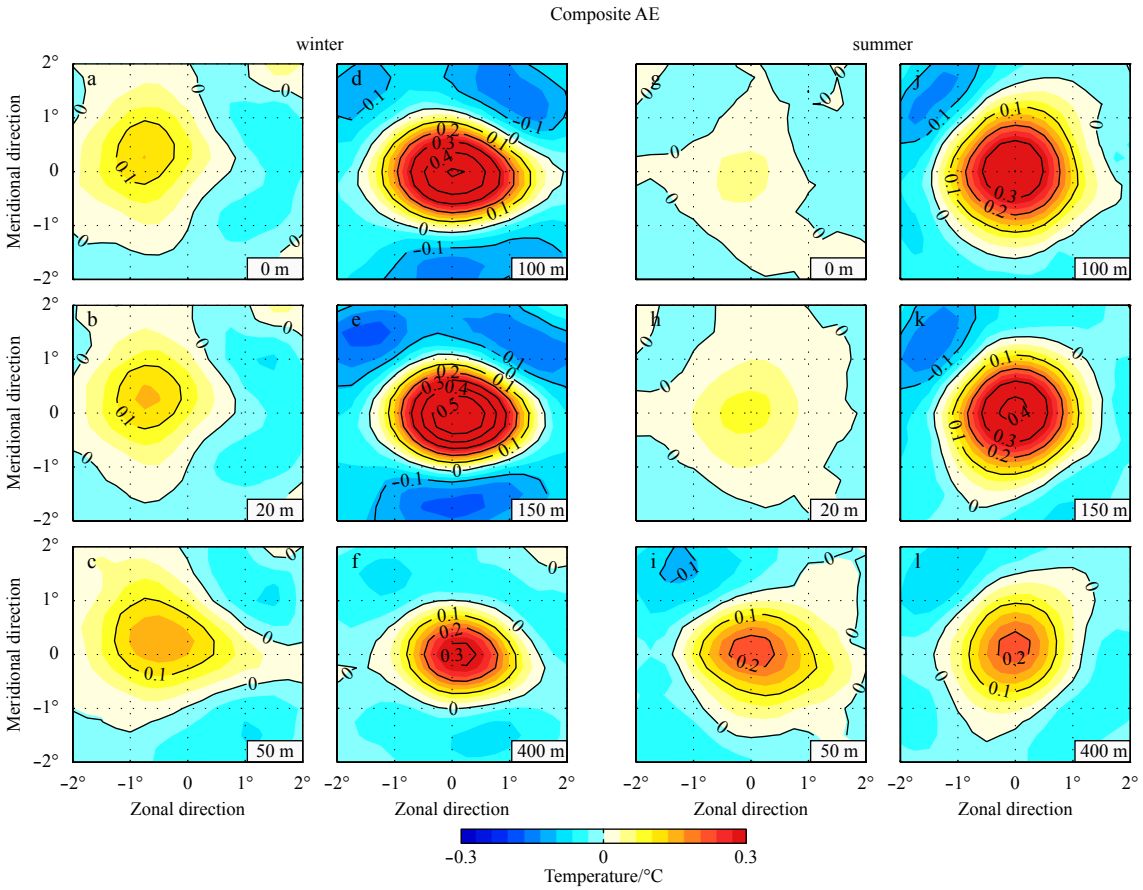

Fig. 2. Composites of horizonal distribution of the temperature anomalies (°C) associated with AEs at different depths. The left two columns are for winter and the right two are for summer. The number in the bottom right corner of each composite map is the water depth of that layer. Contour interval is 0.1°C. The *X*-axes and *Y*-axes in the composite maps indicate the latitudinal and meridional distances (°) from the center of eddy, respectively. The positive directions are eastward and northward, respectively.

omaly associated with AE deviate to the west side of the eddy, and a cold anomaly, though relatively weak, appears on the west side, making the distribution of the temperature anomaly more of a dipole pattern (Fig. 2a)—consistent with the findings of Sun et al. (2016). Similar characteristics can also be found in temperature anomalies in upper layers associated with CEs in winter, except that the asymmetry of the cold anomalies (Figs 3a–c) is not as obvious as that of AEs.

To better understand temperature structure of eddies, composite maps of vertical distribution of temperature anomalies are

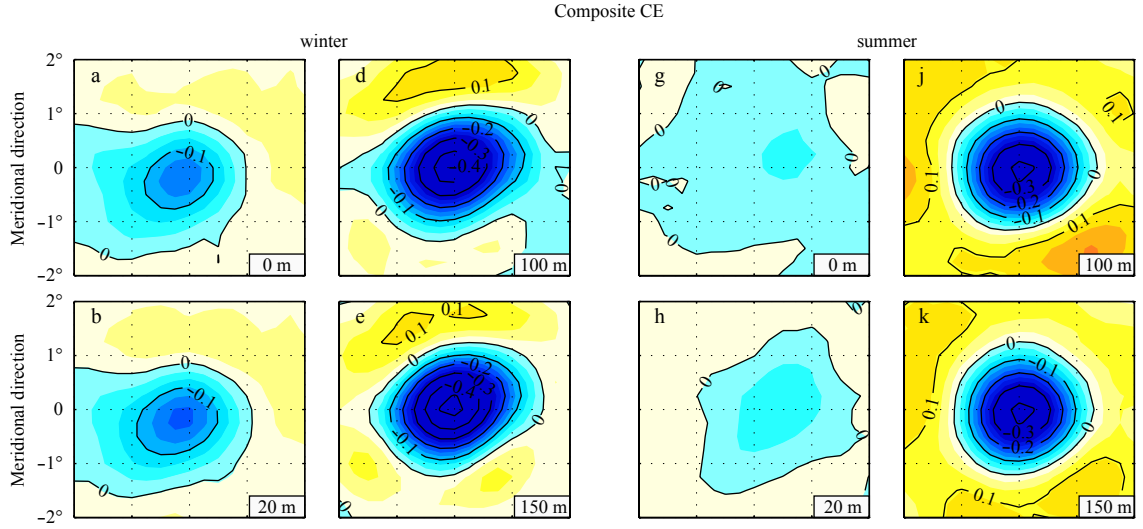

Fig. 3.

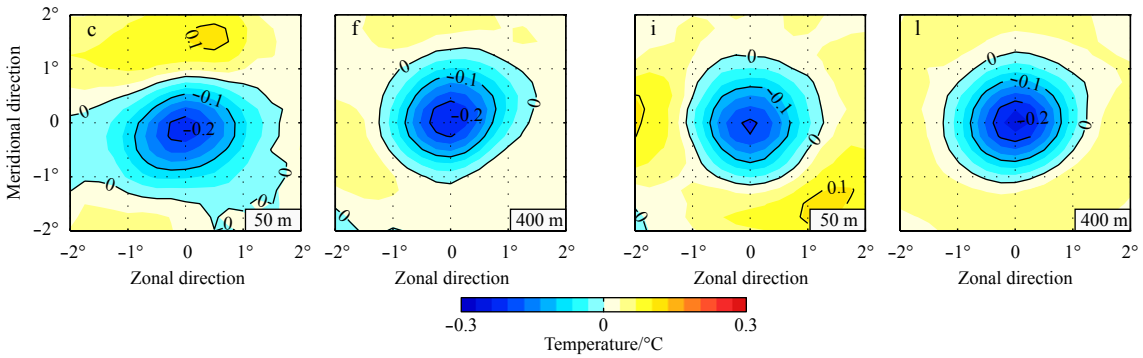

Fig. 3. Composites of horizonal distribution of the temperature anomalies (°C) associated with CEs at different depths. The left two columns are for winter and the right two are for summer. The number in the bottom right corner of each composite map is the water depth of that layer. Contour interval is 0.1°C. The *X*-axes and *Y*-axes in the composite maps indicate the latitudinal and meridional distances (°) from the center of eddy, respectively. The positive directions are eastward and northward, respectively.

plotted (Fig. 4). It can be seen that, in general, the vertical distribution patterns of temperature anomaly induced by AEs and CEs are similar, and both reach their maximum values at 150 m, except that AEs cause positive anomalies whereas CEs induce negative ones (Figs 4a–d). However, if check the layers shallower than 50 m carefully, we can find that the distribution patterns of winter and summer are quite different—the anomalies on the east side and the west side in summer are centrosymmetric (Figs 4f and h), while those in winter manifest a dipolar feature, with positive anomaly on one side and negative anomaly on the other side (Figs 4e and g).

3.2 *Salinity structure*

Using the same method as for temperature analysis, we can

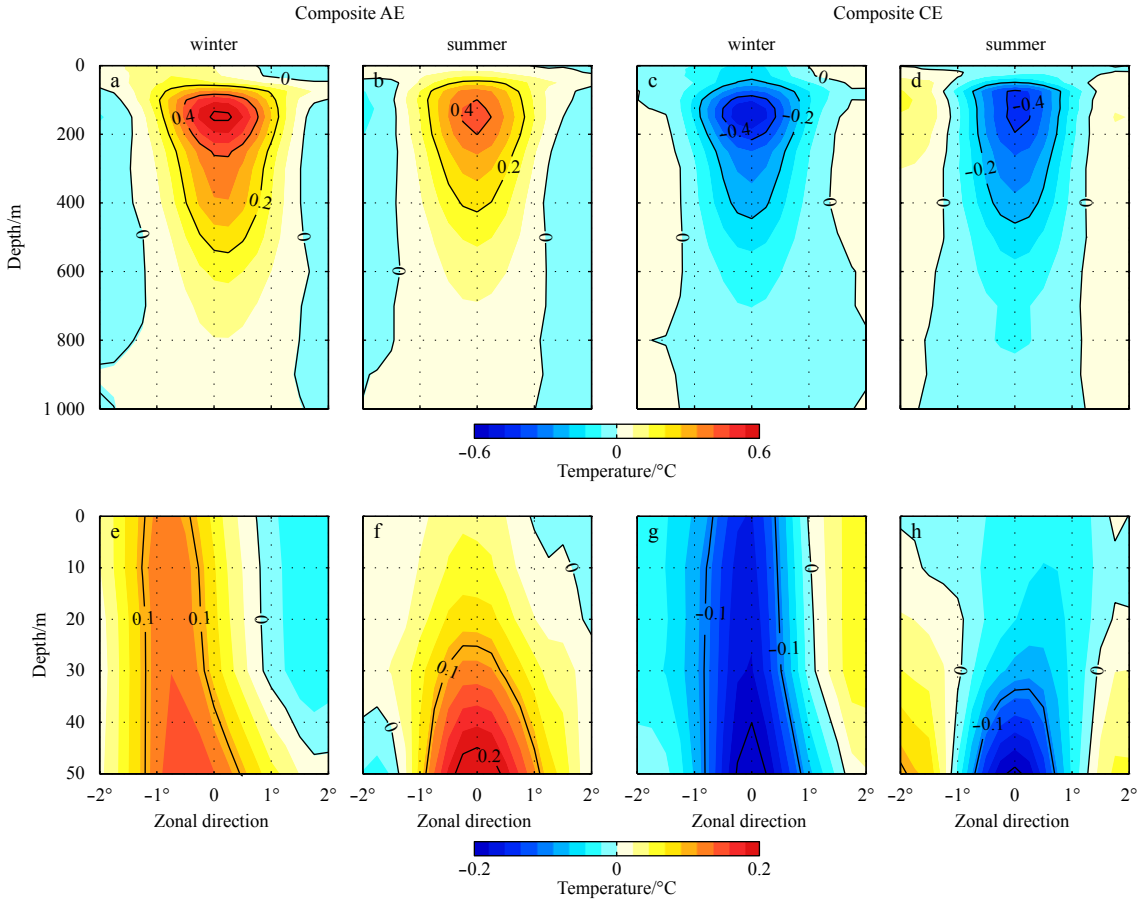

Fig. 4. West-east sections of temperature anomaly (°C) across the eddy center in winter and summer. The upper four panels cover the water column from 0 to 1 000 m, and the lower four panels show the details of 0–50 m of the upper panels. Contour intervals of upper and lower panels are 0.2°C and 0.1°C, respectively. The *X*-axes in the composite maps indicate the latitudinal distances (°) from the center of eddy. The positive direction is eastward.

obtain the composite maps of eddy-induced salinity anomaly (Figs 5–7). We can see that the distribution patterns of salinity anomalies in winter are very similar to those of temperature anomalies. For the layers at 100 m or deeper, the location of maximum salinity anomaly in each layer coincide with the eddy center, and the patterns of anomalies are centrosymmetric. But for the layers at 50 m or shallower, the anomalies in winter are asymmetric and show more of a dipole pattern (Figs 5a–c and 6a–c). For example, the anomaly induced by AEs in surface layer (Fig. 5a) shows a negative pole on the west side of eddy and a positive pole on the

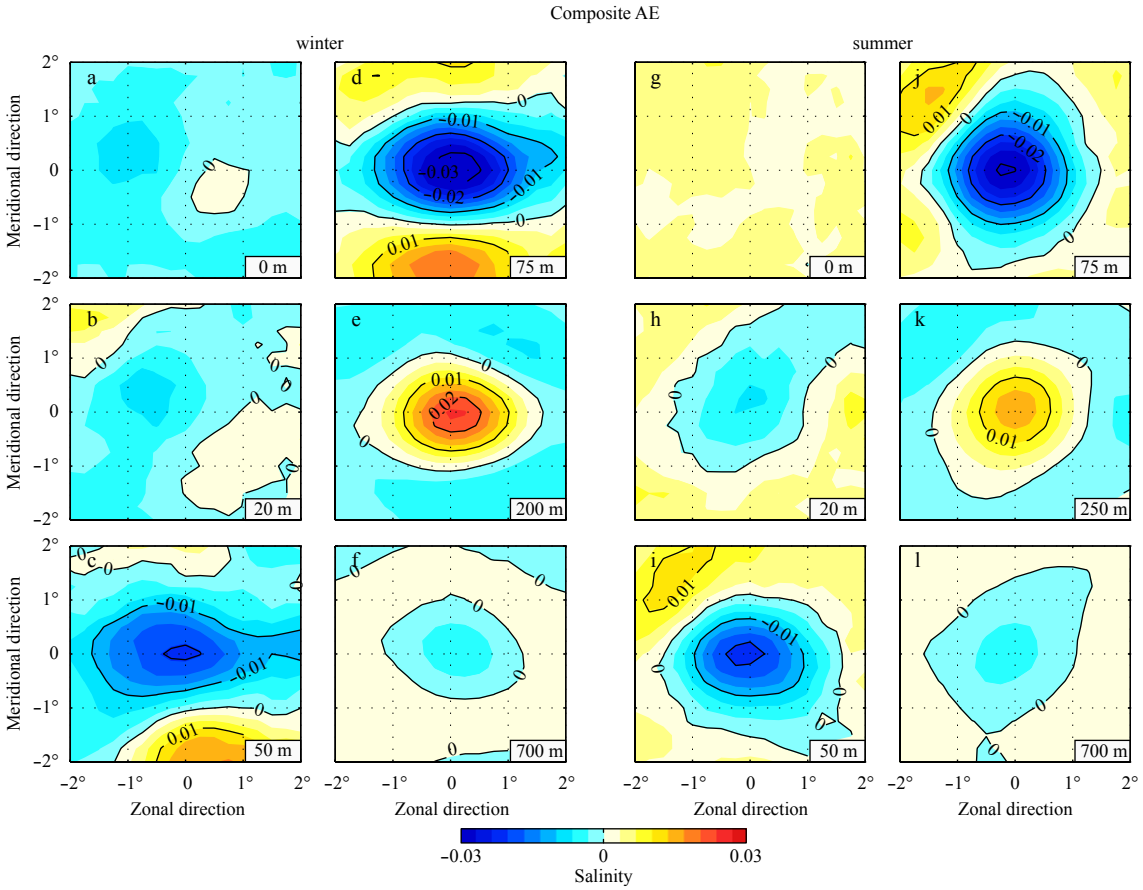

Fig. 5. Composites of horizonal distribution of the salinity anomalies associated with AEs at different depths. The left two columns are for winter and the right two are for summer. The number in the bottom right corner of each composite map is the water depth of that layer. Contour interval is 0.01. The *X*-axes and *Y*-axes in the composite maps indicate the latitudinal and meridional distances (°) from the center of eddy, respectively. The positive directions are eastward and northward, respectively.

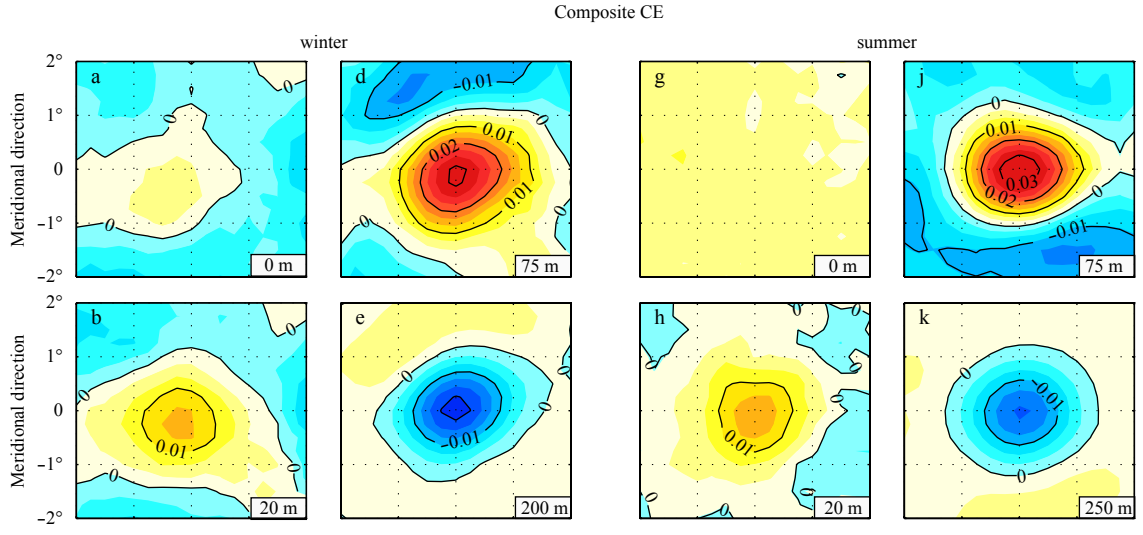

Fig. 6.

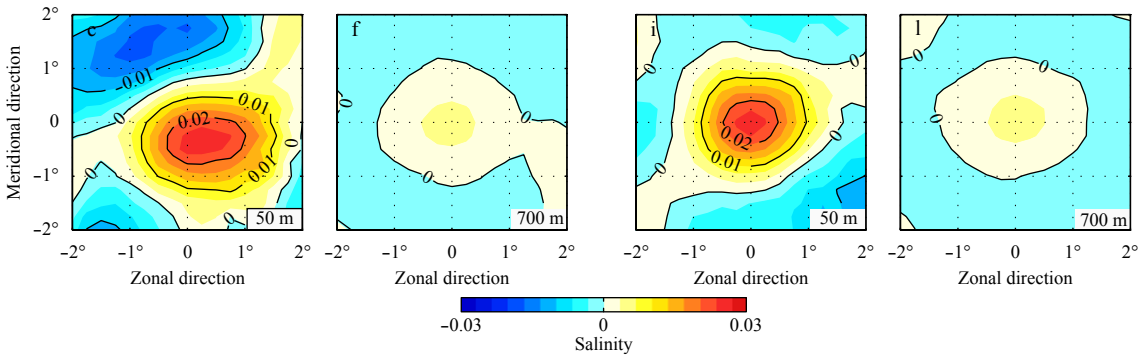

Fig. 6. Composites of horizonal distribution of the salinity anomalies associated with CEs at different depths. The left two columns are for winter and the right two are for summer. The number in the bottom right corner of each composite map is the water depth of that layer. Contour interval is 0.01. The *X*-axes and *Y*-axes in the composite maps indicate the latitudinal and meridional distances (°) from the center of eddy, respectively. The positive directions are eastward and northward, respectively.

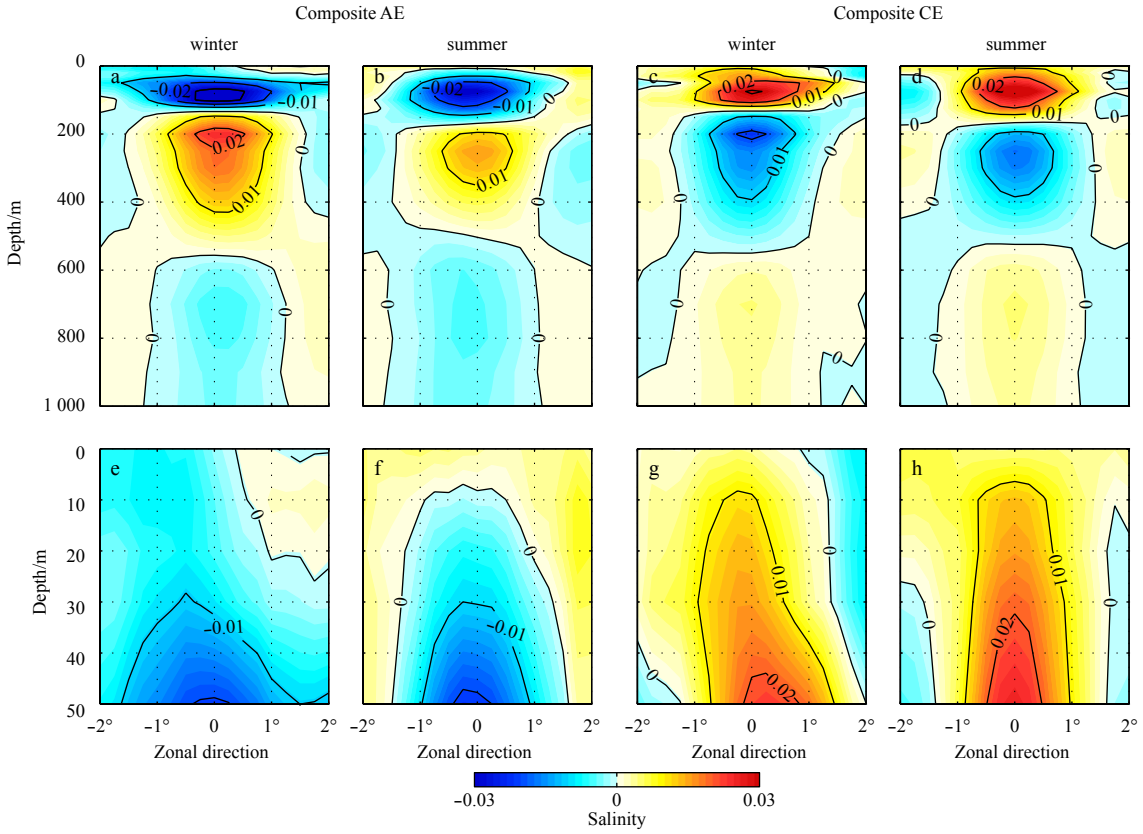

Fig. 7. West-east sections of salinity anomaly across the eddy center in winter and summer. The upper four panels cover the water column from 0 to 1 000 m, and the lower four panels show the details of 0–50 m of the upper panels. Contour interval is 0.01. The *X*-axes in the composite maps indicate the latitudinal distances (°) from the center of eddy. The positive direction is eastward.

east side. Similar pattern can also be found in the layer at 20 m. The asymmetry of salinity anomalies in shallower layers in winter can also be found in Figs 7e and g.

In summer, the centers of eddy-induced salinity anomalies all coincide with eddy center through entire water column. Interestingly, the eddy-induced salinity anomalies at sea surface are all homogeneously positive no matter if the anomaly is associated with AEs or CEs (Figs 5g and 6g). Compared to the vertical distribution of temperature anomalies shown in Figs 4a–d, a salient feature of salinity anomalies is their triple-layer structure - negative-positive-negative for AEs (Figs 7a and b) and positive-negative-positive for CEs (Figs 7c and d), with maximal anomalies occuring at 75 m, 200 m in winter/250 m in summer, and 700 m, respectively.

4 Mechanism of thermohaline structure formation

In the interior of ocean, the low frequency change of local TS can be expressed as

$$\frac{\partial A}{\partial t} + V \cdot \nabla A + w \frac{\partial A}{\partial z} = k_A \Delta A,$$

where A is temperature or salinity, $\boldsymbol{V}$ and w are horizontal velocity vector and vertical velocity associated with eddy, respectively, and k_A is diffusivity coefficient. Therefore, the change of local temperature and salinity, $\frac{\partial A}{\partial t}$, is dominated by horizontal advection term $\boldsymbol{V}\cdot\nabla A$ and vertical advection term $w\frac{\partial A}{\partial z}$, because the diffusion term $k_A\Delta A$ is a minor term compared with the other three. Since $\frac{\partial A}{\partial z}$ can be roughly treated as a constant at a certain depth within an eddy, and theoretically the horizontal distribution of w is centrosymmetric, the distribution pattern of the anomaly resulted from vertical advection $w\frac{\partial A}{\partial z}$ is expected to be also centrosymmetric. However, the anomaly caused by horizontal advection $\boldsymbol{V}\cdot\nabla A$ cannot be centrosymmetric, because ∇A cannot be centrosymmetric. In an idealized two-dimensional temperature/salinity field whose gradient is uniform, the advection on the west side of an AE carries warm water from the south to the north and thus causes a warm anomaly in that region, while on the eddy's east side, cold water flows to the south and a cold anomaly thus appears (Fig. 8a). In this idealized case, the resulted anomaly exhibits a dipole pattern. For a CE, the advection will induce a similar dipole pattern, but in opposite sign (Fig. 8b). Therefore, whether the pattern of the total anomaly associated with an eddy is centrosymmetric or not depends largely on the balance between the vertical advection and the horizontal advection.

Since the thermohaline distribution is very complicated in the SCS and shows remarkable seasonality, it is necessary to investigate the vertical and seasonal variation of horizontal advection. At a certain depth, we first calculate the horizontal advection term of an eddy at each grid point in the 2°×2° area where the eddy is located, then exact same calculation is done for all eddies. After that, we average all the values by seasons and thus get the mean value of horizontal advection at that depth for each season (winter/summer). By repeating the above procedure at each depth, the vertical variation of mean horizontal advection of TS can be obtained and the results are shown in Fig. 9. One of important features in Fig. 9 is that the magnitude of advection decreases dramatically in the layers deeper than 200 m—this is expected because both geostrophic velocity of eddy and horizontal gradient of background temperature/salinity decrease rapidly below 200 m (figures not shown). For the layers shallower than 200 m, the variation of advection is more complicated and shows remarkable seasonality. A common feature of it is that the advection in each of the upper three layers in summer is significantly

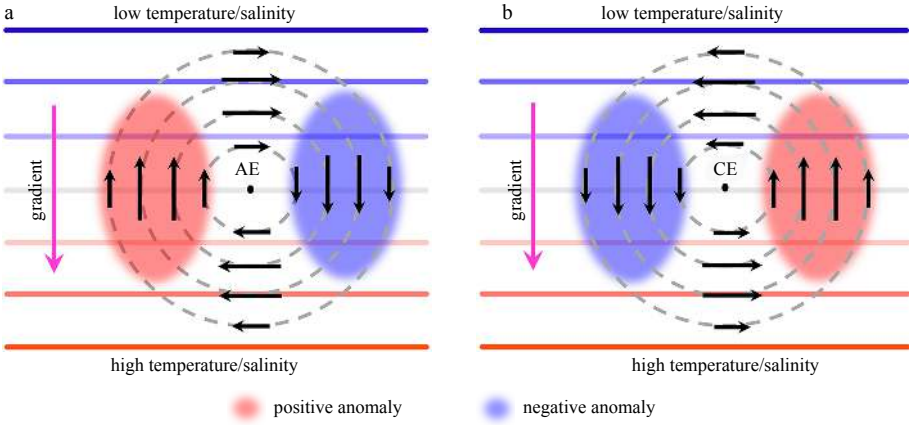

Fig. 8. Schematic diagram of the effects of horizontal advection in a non-homogenous background temperature/salinity field.

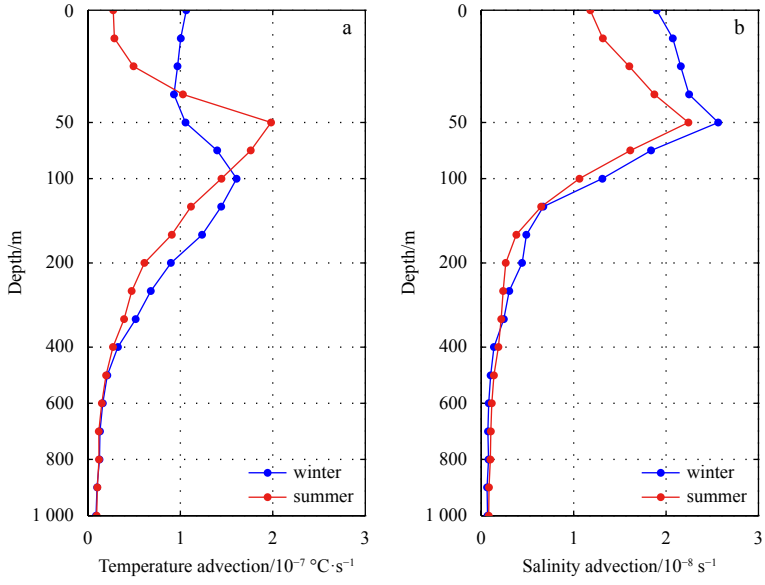

Fig. 9. Vertical variation of mean horizontal advection of temperature (a) and salinity (b) in winter and summer.

weaker than that in winter. This is because the horizontal gradient of background TS in summer in the SCS is much smaller (Figs 10a, d, g and j).

In winter, the temperature in surface layer in the SCS is cold in the north and warm in the south (Fig. 10a), so the temperature gradient is very strong, implying a strong horizontal advection. In addition, both w and $\frac{\partial A}{\partial z}$ in the surface layer are close to zero, or the vertical advection is weak. Thus in the surface layer the horizontal advection is dominant. The above situation is just like the one illustrated by Fig. 8, so the temperature anomalies induced by eddies should be similar to those demonstrated in Fig. 8 if our theory is correct. Composite map (Fig. 2a) does show such a dipolar anomaly similar to the one in Fig. 8a, but it is worth to note that the warm pole of the anomaly is stronger than the cold pole. This is because the downwelling associated with AEs, though very weak in surface layer, still can warms up the surface water, which enhances the warm anomaly and weakens the cold anomaly. The dipole-like asymmetric pattern also exists in the 20 m layer (Fig. 2b), but the anomaly in 50 m layer is neither dipolar nor centrosymmetric (Fig. 2c) but somewhere in between—this is not surprising because the vertical advection enhances rapidly and plays a more dominant role as water depth increases. At 100 m depth, where vertical temperature gradient is around 0.07°C/m (Fig. 11a), if w is estimated with a typical value of 0.2 mm/s, then the magnitude of $w\frac{\partial A}{\partial z}$ is about 1.4×10^{-6}°C/s —one order higher than the horizontal advection. Therefore, even the horizontal advection reaches its maximum at 100 m (Fig. 9a), its role still can be ignored compared with the vertical advection, and the temperature anomaly is expected to be centrosymmetric (Fig. 2d). For deeper layers, the vertical advection is even more dominant as the horizontal advection effects decrease dramatically as water depth increases.

In summer, the temperature in surface layer (Fig. 10d) and 20 m layer (not shown) tend to be homogenous in the entire SCS basin, so the horizontal advection is very weak (Fig. 9a). So, the vertical advection, though weak compared with that in deeper layers, may play a dominant role and generate weak but centrosymmetric temperature anomalies (Figs 2g and h).

The above mechanism can also be used to explain the strength and distribution pattern of the temperature anomalies associated with CEs, and the salinity anomalies also. But one must be careful when apply the mechanism to the salinity anomaly in surface layer, because evaporation/precipitation might be so important in a particular season. Due to the warm and evenly distributed surface temperature (Figs 10d and 11a) and strong monsoonal winds, the evaporation in the SCS is strong and precipitation is less, causing the highest salinity in surface layer among the four seasons (Fig. 11b). In this season, evaporation above the AEs will be further enhanced because of warmer sur-

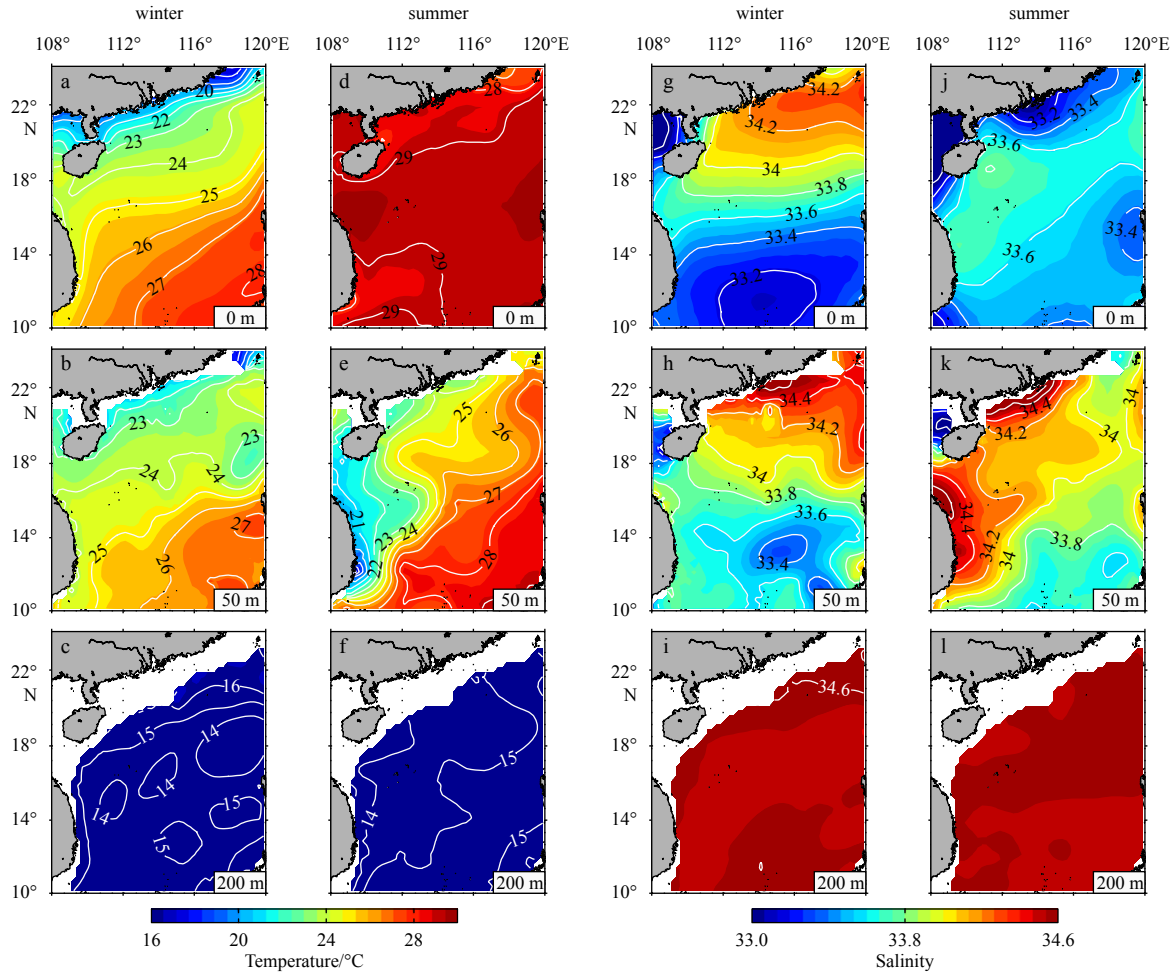

Fig. 10. Horizonal distributions of background temperature (°C) and salinity at different depths (0 m, 50 m, 200 m). Contour intervals for temperature and salinity are 1°C and 0.2, respectively.

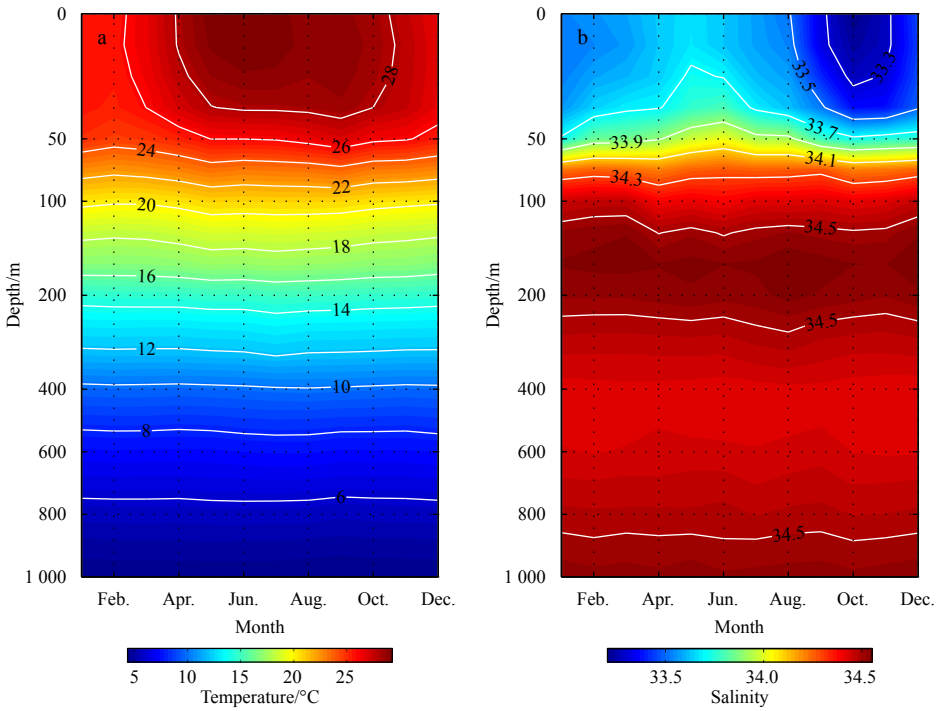

Fig. 11. Seasonal variation of mean temperature (a) and mean salinity (b) averaged in the area deeper than 1 000 m in the SCS. Contour intervals of temperature and salinity are 2°C and 0.2, respectively.

face temperature and stronger surface wind resulted from warmer surface temperature (Sun et al., 2016). The effect of stronger evaporation on salinity is probably much stronger than the one of vertical advection induced by the AEs, which reduces surface salinity. Therefore, the salinity anomaly in Fig. 5g is still positive – in the same sign as the one induced by CEs (Fig. 6g).

The horizontal advection of salinity in upper layers in summer, though smaller than that in winter (Fig. 9b), cannot be ignored and its resulted salinity anomaly should be dipolar if our theory illustrated by Fig. 8 is correct. But why we did not find that dipolar pattern in Fig. 6g? If we look at Fig. 11b carefully, we can find that vertical gradient in summer is much stronger than the other seasons, implying that the vertical advection in this season prevails over horizontal advection and thus the salinity anomaly will be centrosymmetric.

The vertical distribution of temperature anomalies shown in Figs 4a–d is easy to understand as the vertical flow induced by AEs (CEs) transports warm (cold) water downward (upward), thus causes a warm (cold) anomaly below the surface. For salinity, its response to the vertical advection is more complicated because of the existence of maximum salinity at 150 m (Fig. 11b). This unique distribution of background salinity causes the salinity anomaly in the vertical direction exhibit a triple layer structure (Figs 7a–d).

5 Summary

Using the latest eddy dataset and ARMOR3D data, we analyzed the seasonal characteristics of thermohaline structure of mesoscale eddy in the SCS and explored its formation mechanism. Our results show that (1) the horizontal distribution of temperature anomaly induced by eddies is centrosymmetric except in upper layers, where the distribution shows a dipole pattern; (2) the horizontal distribution of salinity anomaly is similar to that of temperature, except that the anomalies in surface layer, no matter in AEs or CEs, are always positive; (3) the vertical distribution of temperature anomaly induced by AEs (CEs) is a single-layer structure with positive (negative) maximum occurring at 150 m, while the salinity anomaly resulted from AEs (CEs) shows a negative-positive-negative (positive-negative-positive) triple-layer structure, with maximal anomalies at 75 m, 200 m in winter/250 m in summer, and 700 m, respectively.

Characteristics of the thermohaline structure associated with eddies in the SCS are mainly determined by the balance of the horizontal and vertical advection of background TS fields. In upper layers (50 m or shallower), the horizontal advection dominates, and thus the pattern of TS anomalies tends to be dipolar; in lower layers, however, the pattern of TS anomalies is centrosymmetric because the vertical advection prevails. It is worth to note that, the vertical advection in summer can also be dominant in the layers close to sea surface as the horizontal gradient of TS in these layers reaches its annual minimum in this season and thus results in a weak horizontal advection. The vertical distribution patterns of TS anomalies associated with eddies are mainly determined by the vertical structure of background TS fields.

Although the mechanism proposed by present study well explains the characteristics and formation of the thermohaline structure associated with eddies in the SCS, the mechanism is largely based on qualitative analysis. It is also worth to note that uncertainties may exist in the composites of eddy thermohaline structure and current field, because the data used in present study are reanalyzed data, whose reliability is partially related to the reanalysis method. Usually, the ideal way to validate the composites is to make comparison with observed eddies in the SCS. However, the eddies in the SCS are quite complicated due to their generation and evolution mechanisms, and this makes the comparison less possible considering the existing observations of eddies are quite limited. Therefore, more detailed quantitative analysis, like the salt and heat budget analysis or numerical sim-

ulation, is still necessary for further validation of the mechanism.

Acknowledgements

The Mesoscale Eddy Trajectory Atlas Product is provided by AVISO+ (http://www.aviso.altimetry.fr/), and Yongcan Zu is also grateful to Dudley B. Chelton for his helpful comments on the dataset. The Global ARMOR3D L4 Reprocessed dataset is provided by Copernicus Marine Environment Monitoring Service (http://marine.copernicus.eu/).

References

Amores A, Melnichenko O, Maximenko N. 2017a. Coherent mesoscale eddies in the North Atlantic subtropical gyre: 3-D structure and transport with application to the salinity maximum. Journal of Geophysical Research: Oceans, 122(1): 23–41, doi: 10.1002/jgrc.v122.1

Amores A, Monserrat S, Melnichenko O, et al. 2017b. On the shape of sea level anomaly signal on periphery of mesoscale ocean eddies. Geophysical Research Letters, 44(13): 6926–6932, doi: 10.1002/2017GL073978

Chelton D B, Schlax M G, Samelson R M, et al. 2007. Global observations of large oceanic eddies. Geophysical Research Letters, 34(15): L15606

Chelton D B, Schlax M G, Samelson R M. 2011. Global observations of nonlinear mesoscale eddies. Progress in Oceanography, 91(2): 167–216, doi: 10.1016/j.pocean.2011.01.002

Chen Gengxin, Hou Yijun, Chu Xiaoqing. 2011. Mesoscale eddies in the South China Sea: Mean properties, spatiotemporal variability, and impact on thermohaline structure. Journal of Geophysical Research: Oceans, 116(6): C06018

Chen Gengxin, Wang Dongxiao, Dong Changming, et al. 2015. Observed deep energetic eddies by seamount wake. Scientific Reports, 5: 17416, doi: 10.1038/srep17416

Dong Changming, McWilliams J C, Liu Yu, et al. 2014. Global heat and salt transports by eddy movement. Nature Communications, 5: 3294, doi: 10.1038/ncomms4294

Faghmous J H, Frenger I, Yao Yuanshun, et al. 2015. A daily global mesoscale ocean eddy dataset from satellite altimetry. Scientific Data, 2: 150028, doi: 10.1038/sdata.2015.28

Falkowski P G, Ziemann D, Kolber Z, et al. 1991. Role of eddy pumping in enhancing primary production in the ocean. Nature, 352(6330): 55–58, doi: 10.1038/352055a0

Fang Yue, Fang Guohong, Yu Kejun. 1996. ADI barotropic ocean model for simulation of Kuroshio intrusion into China southeastern waters. Chinese Journal of Oceanology and Limnology, 14(4): 357–366, doi: 10.1007/BF02850557

Fang Guohong, Wang Gang, Fang Yue, et al. 2012. A review on the South China Sea western boundary current. Acta Oceanologica Sinica, 31(5): 1–10, doi: 10.1007/s13131-012-0231-y

Frenger I, Münnich M, Gruber N, et al. 2015. Southern Ocean eddy phenomenology. Journal of Geophysical Research: Oceans, 120(11): 7413–7449, doi: 10.1002/2015JC011047

Gaube P, McGillicuddy D J Jr, Chelton D B, et al. 2014. Regional variations in the influence of mesoscale eddies on near-surface chlorophyll. Journal of Geophysical Research: Oceans, 119(12): 8195–8220, doi: 10.1002/2014JC010111

Guinehut S, Le Traon P Y, Larnicol G, et al. 2004. Combining Argo and remote-sensing data to estimate the ocean three-dimensional temperature fields—a first approach based on simulated observations. Journal of Marine Systems, 46(1–4): 85–98

Guinehut S, Dhomps A L, Larnicol G, et al. 2012. High resolution 3-D temperature and salinity fields derived from in situ and satellite observations. Ocean Science, 8(5): 845–857, doi: 10.5194/os-8-845-2012

Hu Jianyu, Gan Jianping, Sun Zhenyu, et al. 2011. Observed three-dimensional structure of a cold eddy in the southwestern South China Sea. Journal of Geophysical Research: Oceans, 116(5): C05016

Hu Zifeng, Tan Yehui, Song Xingyu, et al. 2014. Influence of mesoscale eddies on primary production in the South China Sea during spring inter-monsoon period. Acta Oceanologica Sinica, 33(3): 118–128, doi: 10.1007/s13131-014-0431-8

Huang Bangqin, Hu Jun, Xu Hongzhou, et al. 2010. Phytoplankton community at warm eddies in the northern South China Sea in winter 2003/2004. Deep Sea Research Part II: Topical Studies in Oceanography, 57(19–20): 1792–1798

Klein P, Lapeyre G. 2009. The oceanic vertical pump induced by mesoscale and submesoscale turbulence. Annual Review of Marine Science, 1: 351–375, doi: 10.1146/annurev.marine.010908.163704

Mason E, Pascual A, Gaube P, et al. 2017. Subregional characterization of mesoscale eddies across the Brazil-Malvinas confluence. Journal of Geophysical Research: Oceans, 122(4): 3329–3357, doi: 10.1002/2016JC012611

Mulet S, Rio M H, Mignot A, et al. 2012. A new estimate of the global 3D geostrophic ocean circulation based on satellite data and in-situ measurements. Deep Sea Research Part II: Topical Studies in Oceanography, 77–80: 70–81

Nan Feng, He Zhigang, Zhou Hui, et al. 2011. Three long-lived anticyclonic eddies in the northern South China Sea. Journal of Geophysical Research: Oceans, 116(C5): C05002

Shu Yeqiang, Xiu Peng, Xue Huijie, et al. 2016. Glider-observed anticyclonic eddy in northern South China Sea. Aquatic Ecosystem Health & Management, 19(3): 233–241

Small R J, De Szoeke, Xie Shangping, et al. 2008. Air-sea interaction over ocean fronts and eddies. Dynamics of Atmospheres and Oceans, 45(3–4): 274–319

Sun Shuangwen, Fang Yue, Liu Baochao, et al. 2016. Coupling between SST and wind speed over mesoscale eddies in the South China Sea. Ocean Dynamics, 66(11): 1467–1474, doi: 10.1007/s10236-016-0993-4

Wang Dongxiao, Xu Hongzhou, Lin Jing, et al. 2008. Anticyclonic eddies in the northeastern South China Sea during winter 2003/2004. Journal of Oceanography, 64(6): 925–935, doi: 10.1007/s10872-008-0076-3

Wang Qiang, Zeng Lili, Zhou Weidong, et al. 2015. Mesoscale eddies cases study at Xisha waters in the South China Sea in 2009/2010. Journal of Geophysical Research: Oceans, 120(1): 517–532, doi: 10.1002/2014JC009814

Wyrtki K. 1961. Physical Oceanography of the Southeast Asian Waters. UC San Diego: Scripps Institution of Oceanography, 144–182

Zhang Zhengguang, Wang Wei, Qiu Bo. 2014. Oceanic mass transport by mesoscale eddies. Science, 345(6194): 322–324, doi: 10.1126/science.1252418

Zhang Zhiwei, Tian Jiwei, Qiu Bo, et al. 2016. Observed 3D structure, generation, and dissipation of oceanic mesoscale eddies in the South China Sea. Scientific Reports, 6: 24349, doi: 10.1038/srep24349

Zu Tingting, Wang Dongxiao, Yan Changxiang, et al. 2013. Evolution of an anticyclonic eddy southwest of Taiwan. Ocean Dynamics, 63(5): 519–531, doi: 10.1007/s10236-013-0612-6